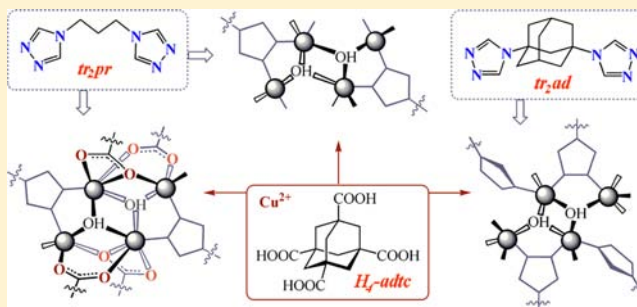


Functionalized Adamantane Tectons Used in the Design of Mixed-Ligand Copper(II) 1,2,4-Triazolyl/Carboxylate Metal–Organic Frameworks

Ganna A. Senchyk,[†] Andrey B. Lysenko,^{*,†} Harald Krautscheid,[‡] Eduard B. Rusanov,[§] Alexander N. Chernega,[§] Karl W. Krämer,[⊥] Shi-Xia Liu,^{*,⊥} Silvio Decurtins,[⊥] and Konstantin V. Domasevitch[†][†]Inorganic Chemistry Department, Taras Shevchenko National University of Kyiv, Volodimirska Street 64, Kyiv 01033, Ukraine[‡]Institut für Anorganische Chemie, Universität Leipzig, Johannisallee 29, D-04103 Leipzig, Germany[§]Institute of Organic Chemistry, Murmanska Street 5, Kyiv 02660, Ukraine[⊥]Département für Chemie und Biochemie, Universität Bern, Freiestrasse 3, CH-3012 Bern, Switzerland

S Supporting Information

ABSTRACT: Bistriazoles, 1,3-bis(1,2,4-triazol-4-yl)propane (**tr₂pr**) and 1,3-bis(1,2,4-triazol-4-yl)adamantane (**tr₂ad**), were examined in combination with the rigid tetraprotic 1,3,5,7-adamantanetetracarboxylic acid (**H₄-adtc**) platform for the construction of neutral heteroleptic copper(II) metal–organic frameworks. Two coordination polymers, [$\text{Cu}_4(\text{OH})_2(\text{H}_2\text{O})_2$] $\{\text{Cu}_4(\text{OH})_2\}(\text{tr}_2\text{pr})_2(\text{H-adtc})_4 \cdot 2\text{H}_2\text{O}$ (**1**) and [$\text{Cu}_4(\text{OH})_2(\text{tr}_2\text{ad})_2(\text{H-adtc})_2(\text{H}_2\text{O})_2$] $\cdot 3\text{H}_2\text{O}$ (**2**), were synthesized and structurally characterized. In complexes **1** and **2**, the N^1, N^2 -1,2,4-triazolyl (**tr**) and μ_3 -OH[−] groups serve as complementary bridges between adjacent metal centers supporting the tetranuclear dihydroxo clusters. The structure of **1** represents a unique association of two different kinds of centrosymmetrical $\{\text{Cu}_4(\text{OH})_2\}$ units in a tight 3D framework, while in compound **2**, another configuration type of acentric tetranuclear metal clusters is organized in a layered 3,6-hexagonal motif. In both cases, the $\{\text{Cu}_4(\text{OH})_2\}$ secondary building block and trideprotonated carboxylate **H-adtc**^{3−} can be viewed as covalently bound six- and three-connected nodes that define the net topology. The **tr** ligands, showing μ_3 - or μ_4 -binding patterns, introduce additional integrating links between the neighboring $\{\text{Cu}_4(\text{OH})_2\}$ fragments. A variable-temperature magnetic susceptibility study of **2** demonstrates strong antiferromagnetic intracenter coupling ($J_1 = -109 \text{ cm}^{-1}$ and $J_2 = -21 \text{ cm}^{-1}$), which combines for the bulk phase with a weak antiferromagnetic intercluster interaction ($zJ = -2.5 \text{ cm}^{-1}$).



■ INTRODUCTION

The engineering of metal–organic coordination solids,¹ built upon secondary building units (SBUs), tends to be the most rapidly investigated area with an enormous potential for many practical applications.² In this context, the main efforts are centered around the ligand design concept that includes the use of functionalized symmetrical multitopic building blocks for the rational control of their self-assembly with SBUs. Adamantane derivatives represent very promising scaffolds for fabrication of a prototype ligand family with desirable donors having angular, tripodal, or tetrahedral binding orientations.^{3–6} Recently, we developed a convenient route to a big library of 1,2,4-triazole-functionalized adamantane tectons to be employed toward metal–organic frameworks (MOFs).⁷ The neutral 1,2,4-triazole derivatives demonstrate an attractive feature to combine metal centers in discrete polynuclear fragments of various configurations (di-, tri-, and tetranuclear units, etc.).⁸ At the same time, the ability of anionic adamantane polycarboxylates as

suitable complementary cobridges offers a straightforward mixed-ligand approach to the neutral and highly stable frameworks, e.g., in which the adamantane scaffold would result in an overall stiffening of the structural motifs. Triazoles and carboxylates can play a similar coordination role, reaching a high degree of preorganization in the metal cluster assembly. On the other hand, the ability to control electronic and magnetic interactions between paramagnetic metal centers is of fundamental importance.⁹ The magnetic exchange interactions are known to be dependent on the nature of the short bridges (oxalate, carboxylate, cyanide, and azole heterocycles) connecting the paramagnetic ions in polynuclear clusters. The 1,2,4-triazole/carboxylate functional groups provide different types of magnetic exchange between the metal centers, and their combination in one compound is often a prerequisite for

Received: September 16, 2012

Published: January 7, 2013

strong magnetic coupling.¹⁰ Such a “mixed-ligand” approach based on the complementary role of *N,N*-azoles with short inorganic or organic bridges seems to be promising for the cluster design with their further organization in MOFs and for obtaining novel magnetic materials,¹¹ preferentially exhibiting a long-range-ordered magnetic phase.^{11f} In this work, we employed tetrafunctional adamantanecarboxylic acid (**H₄-adtc**) in combination with bistriazole ligands (**tr₂pr** and **tr₂ad**) for the construction of novel Cu^{II} MOFs based on discrete coordination clusters.

EXPERIMENTAL SECTION

Synthesis of the Organic Ligands. All chemicals were of reagent-grade and were used as received without further purification. The 1,2,4-triazole ligands were prepared in yields of up to 60% by refluxing of the corresponding diamines (propane-1,3-diamine and adamantane-1,3-diamine) with *N,N*-dimethylformamide azine in xylene/toluene in the presence of *p*-toluenesulfonic acid monohydrate as the catalyst.^{7a,b} Adamantane-1,3,5,7-tetracarboxylic acid was synthesized via photochemical cyanation¹² followed by hydrolysis.^{7c}

Synthesis of the Coordination Compounds. All complexes were prepared under hydrothermal conditions as follows. A mixture of the starting compounds and 5 mL of distilled water were placed into a 20 mL Teflon-lined stainless steel autoclave, stirred for 30 min, and heated at 180 °C for 40 h in an oven, with further cooling to room temperature (cooling rate 2.5 °C h⁻¹). The crystalline products were collected, washed with water and methanol, and dried in air.

[Cu₄(OH)₂(H₂O)₂](Cu₄(OH)₂(tr₂pr)₂(H-adtc)₄·2H₂O (1). A mixture of Cu(OAc)₂·H₂O (22.5 mg, 0.112 mmol), tr₂pr (10.0 mg, 0.056 mmol), and H₄-adtc (17.5 mg, 0.056 mmol) in a 2:1:1 molar ratio and 5 mL of water were placed in a Teflon reactor and heated at 180 °C for 40 h. Cooling to room temperature for 60 h leads to a mixture containing dark-blue prisms of the main product and minor amounts of light-green needles of unknown composition. The desired prisms were separated in 31 mg yield (50%) by a flotation method (differences in density) in a CHBr₃/CHCl₃ solution. Anal. Calcd for C₇₀H₈₄Cu₈N₁₂O₄₀: C, 37.50; H, 3.78; N, 7.50. Found: C, 37.61; H, 3.67; N, 7.58. IR (KBr disks, selected bands, cm⁻¹): 425w, 490w, 534w, 637m, 679m, 728m, 875m, 1058m, 1185m, 1190s, 1340vs, 1370vs, 1456m, 1570vs, 1690s, 1717s, 2855m, 1906m, 2940m, 3147m.

[Cu₄(OH)₂(tr₂ad)₂(H-adtc)₂(H₂O)₂·3H₂O (2). A mixture of Cu(OAc)₂·H₂O (14.8 mg, 0.074 mmol), tr₂ad (10.0 mg, 0.037 mmol), and H₄-adtc (11.6 mg, 0.037 mmol) in a 2:1:1 molar ratio and 5 mL of water were placed in a Teflon reactor and heated at 180 °C for 40 h. Cooling to room temperature for 60 h leads to green-blue compact crystals of the pure product in 37 mg yield (65%). Anal. Calcd for C₅₆H₇₄Cu₄N₁₂O₂₃: C, 43.75; H, 4.85; N, 10.93. Found: C, 43.57; H, 4.98; N, 10.89. IR (KBr disks, selected bands, cm⁻¹): 424w, 475w, 630m, 660m, 684m, 725s, 1063m, 1150m, 1190s, 1265m, 1324s, 1385vs, 1450m, 1564vs, 1700s, 2070w, 2860s, 2940s, 3120s, 3386s. The crystalline sample prepared under hydrothermal conditions was selected for the magnetic measurements.

A series of experiments aimed at optimizing the reaction conditions were performed in aqueous solutions at reflux. The reaction products were characterized by means of powder X-ray diffraction (PXRD), IR spectrometry, and CHN analysis. In a typical experiment, a reaction mixture of Cu(OAc)₂·H₂O, H₄-adtc, and the corresponding triazole ligands in water with initial metal-to-ligand ratios close to the compositions observed in compounds **1** and **2** was stirred at reflux for more than 30 h (for experimental details, see the Supporting Information, SI). The resulting powdered solids were filtered, washed with water and methanol, and dried at room temperature prior to analysis. The bulk samples prepared in this way were identified as pure phases of **1** and **2**, supported by a match of the experimental PXRD pattern to the theoretical pattern simulated from single-crystal data (Figures S16 and S17 in the SI). However, the utilized hydrothermal conditions given above are more favorable for the preparation of high-quality single crystals of compounds **1** and **2**.

Measurements. Elemental analysis was carried out with a Vario EL-Heraeus microanalyzer. IR spectra (400–4000 cm⁻¹) were collected using a Perkin-Elmer FTIR spectrometer on KBr disks. PXRD was carried out on a Stoe STADIP (Cu Kα₁) using a linear PSD detector and on a Shimadzu XRD-6000 (Cu Kα radiation). The temperature-dependent X-ray measurements were carried out on a Stoe STADIP with a high-temperature attachment and image-plate detector system. Thermogravimetric/differential thermal analysis mass spectrometry (TG/DTA-MS) was carried out on a Netzsch F1 Jupiter device connected to an Aeolos mass spectrometer. The sample was heated at a rate of 10 K min⁻¹. Magnetic susceptibility data were recorded using a Quantum design MPMS-SXL SQUID magnetometer as a function of the field (0.1–5.0 T) and temperature (1.9–300 K). Experimental data were corrected for sample holder and diamagnetic contributions calculated from tabulated values.

X-ray Crystallography. Diffraction data for **1** were collected at 213 K using a Stoe Imaging Plate Diffraction System and at 296 K on a Bruker APEX II CCD area-detector diffractometer (φ scans) for **2** (graphite-monochromated Mo Kα radiation, $\lambda = 0.71073$ Å). The data were corrected for Lorentz-polarization effects and for the effects of absorption (**1**, numerical absorption correction; **2**, multiscan method). The structures were solved by direct methods and refined by full-matrix least squares on F^2 using the SHELX-97 program package.¹³ CH hydrogen atoms were placed in calculated positions and refined as fixed contributions with $U_{\text{iso}} = 1.2U_{\text{eq}}(\text{C})$, while OH hydrogen atoms were localized and then fixed at O–H = 0.85 Å with $U_{\text{iso}} = 1.5U_{\text{eq}}(\text{O})$. Relatively high values for thermal parameters were indicative of possible disorder in the solvent region. The oxygen atoms for one (**1**) and two (**2**) independent solvate water molecules were refined with a partial occupancy factor of 0.5. Crystallographic data and experimental details for structural analyses are summarized in Table 1. The crystallographic material can also be obtained from the CCDC, with the deposition numbers being CCDC 890823 and 890824 (for **1** and **2**, respectively).



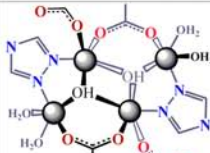
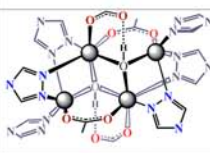

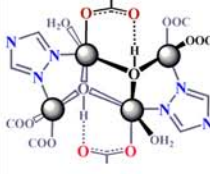

RESULTS AND DISCUSSION

Crystal Structures. The structural characteristics of the copper(II)/tr/carboxylate “mixed-ligand” system were shown to be sensitive to the synthetic conditions (especially the pH influence), giving discrete cluster types with diverse nuclearities and geometries.¹⁴ A rational combination of the short organic

Table 1. Crystal Data for Reported Structures **1** and **2**

	1	2
formula	C ₃₅ H ₄₂ Cu ₄ N ₆ O ₂₀	C ₅₆ H ₇₄ Cu ₄ N ₁₂ O ₂₃
<i>T</i> /K	213	296
<i>M</i>	1120.91	1537.43
cryst syst	triclinic	triclinic
space group, <i>Z</i>	$P\bar{1}$, 2	$P\bar{1}$, 2
<i>a</i> /Å	8.6000(4)	11.3853(4)
<i>b</i> /Å	13.1848(7)	12.0558(4)
<i>c</i> /Å	18.3098(10)	23.4951(9)
α /deg	97.207(6)	93.417(2)
β /deg	101.911(6)	97.951(2)
γ /deg	107.200(6)	109.364(2)
<i>V</i> /Å ³	1901.57(17)	2993.97(18)
$\mu(\text{Mo K}\alpha)/\text{mm}^{-1}$	2.305	1.496
<i>D_c</i> /g cm ⁻³	1.958	1.705
$\theta_{\text{max}}/\text{deg}$	26.02	26.44
measd/unique reflns	15185/7280	28474/12182
param refined	595	855
R1, wR2 [<i>I</i> > 2 σ (<i>I</i>)]	0.035, 0.088	0.049, 0.108
R1, wR2 (all data)	0.044, 0.090	0.088, 0.119
GOF on F^2	0.935	1.016
max, min peak/e Å ⁻³	1.35, -0.56	1.07, -0.53

Table 2. Structural Features of the Triazolyl/Carboxylate Sustaining $\{\text{Cu}_4(\text{OH})_2\}$ Clusters

No	Cluster configuration	Triazole function: number & link mode	Carboxylate function: number & link mode	Ligands & net topology	Ref.
1.		2; $\mu_2\text{-N}^1, \text{N}^2$	2; <i>syn, syn</i> - $\mu_2\text{-}\eta^1: \eta^1$ 2; $\mu_2\text{-}\eta^2: \eta^0$ 2; X=bidentate or terminal	{4-amino-1,2,4-triazole; pivalic acid}, 0D; {3-amino-1,2,4-triazole; trimesic acid}, 3D; {4 <i>H</i> -1,2,4-triazole; trimesic acid}, 3D; {4-amino-1,2,4-triazole; 4-nitrobenzoic acid}, 0D	15 16 10 17
		2; $\mu_2\text{-N}^1, \text{N}^2$	2; <i>syn, syn</i> - $\mu_2\text{-}\eta^1: \eta^1$ 2; $\mu_2\text{-}\eta^2: \eta^0$ 2; X= intercluster-bridge	{3-amino-1,2,4-triazole; benzene-1,2,4,5-tetracarboxylic acid}, 3D {4 <i>H</i> -1,2,4-triazole; benzene-1,2,4-tricarboxylic acid}, 3D	16 17
2.		2; $\mu_2\text{-N}^1, \text{N}^2$	2; <i>syn, syn</i> - $\mu_2\text{-}\eta^1: \eta^1$ 2; $\mu_2\text{-}\eta^2: \eta^0$ (intracore H-bond) 2; bidentate or terminal	{4- <i>tert</i> -butyl-1,2,4-triazole; pivalic acid}, 0D {1,2-bis(1,2,4-triazol-4-yl)ethane; trimesic acid}, 3D	15 18
			2; $\mu_2\text{-N}^1, \text{N}^2$	2; <i>syn, syn</i> - $\mu_2\text{-}\eta^1: \eta^1$ 2; terminal	{4 <i>H</i> -1,2,4-triazole; benzene-1,2,3-tricarboxylic acid}, 3D
3.		2; $\mu_2\text{-N}^1, \text{N}^2$	2; <i>syn, syn</i> - $\mu_2\text{-}\eta^1: \eta^1$ 2; terminal	{4 <i>H</i> -1,2,4-triazole; benzene-1,2,3-tricarboxylic acid}, 3D	17
4.		4; $\mu_2\text{-N}^1, \text{N}^2$	2; <i>syn, syn</i> - $\mu_2\text{-}\eta^1: \eta^1$	{3,5-dimethyl-4-amino-1,2,4-triazole; pivalic acid}, 0D	15
		2; N^1 -terminal	2; terminal (intracore H-bond)		
5.		2; $\mu_2\text{-N}^1, \text{N}^2$	2; <i>syn, syn</i> - $\mu_2\text{-}\eta^1: \eta^1$	{ <i>tr, ad</i> }; trimesic acid}, 3D	19
		2; N^1 -terminal	2; terminal (intracore H-bond) 2; terminal		
6.		2; $\mu_2\text{-N}^1, \text{N}^2$	2; terminal (intracore H-bond) 4; terminal	{ <i>tr, pr</i> ; <i>H, adtc</i> }, compound 1, type A, 3D	this work
			2; $\mu_2\text{-N}^1, \text{N}^2$		
7.		2; $\mu_2\text{-N}^1, \text{N}^2$	4; terminal (intracore H-bond) 2; aniso-bidentate	{ <i>tr, ad</i> ; <i>H, adtc</i> }, compound 2, type C, 2D	this work
			2; N^1 -terminal		

and inorganic bridges demonstrates a high level of self-assembling capacity, preferentially supporting the tetranuclear

dihydroxo unit $\{\text{Cu}_4(\text{OH})_2\}$. However, only five principal types of such clusters are known so far^{10,15–19} (Table 2), and three

new configurations are presented in this work. Upon comparison of the geometrical features, it becomes obvious that N^1, N^2 -tr is a required unit, while the carboxylic group can serve either as an additional bridge or as a terminal ligand, usually being involved in hydrogen-bonding interactions. However, the resulting framework topology mostly depends on the connecting role of the polycarboxylate donor, while triazole acts as a terminal link only in special cases.

The nitrogen-donor ligands used in the present work consist of two 1,2,4-triazolyl termini separated by either a flexible linear $-(CH_2)_3-$ spacer or a rigid angular adamantane scaffold, which preprogram a long separation of ~ 9.0 – 11.5 Å between the metal cluster nodes in the MOFs. Furthermore, in both azole ligands, the aliphatic spacer consists of a three-carbon chain: the principal difference lies in the slenderness of propane and the more rigid shape of the diamondoid skeleton. The tetraprotic H_4 -adtc implements a source of perfect tetrahedral building blocks that accurately dictate the network types.

The hydrothermal reaction of copper(II) acetate with a mixture of tr_2pr and H_4 -adtc leads to the 3D MOF **1**. The coexistence of two related, but slightly different centrosymmetrical $\{Cu_4(\mu_3-OH)_2\}$ clusters is the most striking feature of its structure (types A and B; Figure 1). The tetranuclear

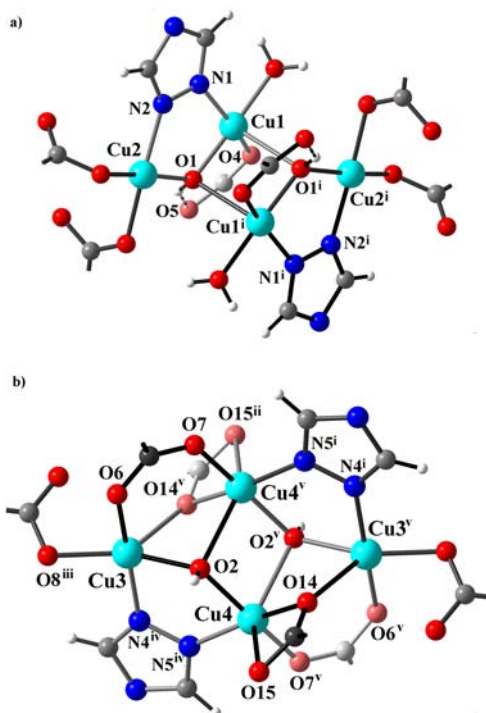


Figure 1. Types A (a) and B (b) of the tetranuclear SBUs observed in compound **1**. Symmetry codes: (i) $-x + 2, -y + 1, -z + 1$; (ii) $-x + 1, -y, -z + 1$; (iii) $-x + 1, -y + 1, -z$; (iv) $x - 1, y - 1, z - 1$; (v) $-x + 1, -y, -z$.

inorganic cores are primarily held by means of either a N^1, N^2 -tr (A) or a carboxylate/ N^1, N^2 -tr (B) bridging combination. In motif A, the Cu1 and Cu2 cations possess distorted square-pyramidal $\{NO_3 + O\}$ and square-planar $\{NO_3\}$ configurations, respectively, which are completed with terminal carboxylates from 3-fold-deprotonated H -adtc $^{3-}$ ligands and water molecules (Figure 1a and Table 2). A strong synergetic cooperation of tr and OH^- bridges promotes a short-distance disposition of the metal ions, while the axial contacts of the hydroxo groups

with the symmetry-related copper ions remain rather long [$O1-Cu1^i = 2.401(2)$ Å; Table 3]. Thus, it seems advisable to consider the $\{Cu_4(\mu_3-OH)_2(\mu_2-tr)_2\}$ fragment as two self-associating $\{Cu_2(\mu_3-OH)(\mu_2-tr)\}$ units fused through two axial positions. The cluster A represents a principally novel and unprecedented structure type where the tetranuclear dihydroxo SBU is supported only by μ_2 -tr and μ_3 - OH^- functions.

The other structural motif B shows close similarity to the known ones that are depicted in Table 2 (cluster nos. 1–3). Thus, the $\{Cu_4(\mu_3-OH)_2\}$ core is maintained by means of N^1, N^2 -tr, *syn, syn*- μ_2 - η^1 : η^2 - COO^- , and *syn, syn*- μ_2 - η^2 : η^1 - COO^- (chelate coordination type) bridges (Figure 1 b and Table 2). Unlike the situation in type A, here both tr and *syn, syn*- COO^- coordinations are especially suitable for assisting the more rigid rhombic cluster with shorter edge distances between the metal ions [$Cu3 \cdots Cu4 = 3.459(1)$ Å and $Cu3 \cdots Cu4^{ii} = 3.197(1)$ Å]. That is a consequence of the powerful binding role of the carboxylates, but nevertheless it does not prevent the cooperative tendency between tr and OH^- groups in generating the longer axial bond $O2-Cu4^v$ [2.421(2) Å]. The same effect is observed in the previously reported compounds (cluster nos. 1–3 from Table 2) and surprisingly disappears in the presence of more than two triazole functional groups. Thus, the coordination arrangement of the copper atoms Cu3 and Cu4 adopts typical square-pyramidal $\{NO_3 + O\}$ and strongly distorted six-coordinated surroundings (owing to the elongated contact with the O15 chelating carboxylate), respectively (Figure 1b and Table 3).

The polytopic carboxylate ligands support the incorporation of both cluster types into the tight 3D framework that can be topologically characterized in two ways. Considering adamantancarboxylate H -adtc $^{3-}$ as an independent 3-connected node, the subtopological motif of the $\{Cu_4(OH)_2\}$ (H -adtc) array can then be classified as a binodal $(3-c)_2(6-c)$ net with the Schläfli notation of $\{4^2.6\}_2\{4^4.6^2.8^7.10^2\}$,²⁰ in which the $\{Cu_4(OH)_2\}$ SBUs are 6-c nodes. Taking into account only polynuclear cluster nodes, the structure appears as a 8-c uninodal net with a sqc117 topological type²¹ $\{3^6.4^{12}.5^8.6^2\}$ (Figure 2b). The $\{Cu_4(OH)_2\}$ units are interlinked with eight others at distances of $A \cdots A = 13.44$ Å, $A \cdots B = 9.88$ – 12.70 Å, and $B \cdots B = 13.19$ Å by carboxylate bridges in such a way that each cluster type is evenly aligned along the three crystallographic axes. tr_2pr as a μ_4 -bitopic mode does not influence the resultant topology and provides only an additional coordination connection between the A and B SBUs at a distance of 9.88 Å.

The configurations of the $\{Cu_4(\mu_3-OH)_2\}$ cluster and the overall network structure can be regulated even through simple changes in the spacer of the bistriazole ligand. Thus, the replacement of the flexible propylene link by the rigid adamantane skeleton in tr_2ad leads to impressive modifications of the structural topology and to novel organizations of the polynuclear fragments. The $\{Cu_4(\mu_3-OH)_2\}$ cluster as a structural node in complex **2** appears to be a unique noncentrosymmetric assembly (type C; Tables 2 and 3 and Figure 3). This unusual motif is facilitated only by N^1, N^2 -tr and μ_3 - OH bridges, but the existence of a monodentate triazole function appreciably influences the geometrical parameters of the unit. In contrast to types A and B of **1**, the configuration of cluster C of **2** becomes closer to that of two triangular $\{Cu_3(\mu_3-OH)\}$ units, sharing a common edge, rather than to self-associating $[Cu_2(\mu_3-OH)(\mu_2-tr)]$ dimers, and thus a relatively narrow Cu–OH bond length distribution is realized [1.956(2)–2.026(2) Å]. Four terminal and two anisobidentate

Table 3. Principal Geometric Parameters of Tetranuclear $\{\text{Cu}_4(\text{OH})_2\}$ Cluster Types Observed in the Structures of 1 and 2

cluster type	type A (1)	type B (1)	type C (2)
coord. environments, Reedijk's factor, τ^{22}	Cu1 $\{\text{NO}_3 + \text{O}\}$, 0.20 Cu2 $\{\text{NO}_3\}$, 0.06	Cu3 $\{\text{NO}_3 + \text{O}\}$, 0.17 Cu4 $\{\text{NO}_3\}$	Cu1 and Cu4 $\{\text{N}_2\text{O}_4\}$ Cu2 $\{\text{NO}_3 + \text{O}\}$, 0.14 Cu3 $\{\text{NO}_3 + \text{N}\}$, 0.24
Cu–N, N^1, N^2 -tr	1.988(3)–2.009(3)	1.983(3)–1.997(3)	1.981(3)–1.988(3), 2.271(3)–2.334(3)
Cu–N, $\text{tr}_{\text{terminal}}$			1.989(3)–2.006(3)
Cu–O _{syn,syn-COO⁻}		1.934(2)–1.988(2)	
Cu–O _{chelate-bridging COO⁻}		1.960(2), 2.446(2), 2.495(3)	
Cu–O _{anisobidentate COO⁻}			1.988(3), 2.691(3) 1.985(3), 2.685(3)
Cu–O _{terminal COO⁻}	1.915(2)–1.945(2)	1.983(3)	1.905(2)–1.955(2)
Cu–O _{water}	1.943(2)		2.279(3)–2.469(3)
Cu–O(H)–Cu	1.902(2)–1.914(2), 2.401(2)	1.944(2)–1.958(2), 2.421(2)	1.956(2)–2.026(2)
$\text{Cu}\{N^1, N^2\text{-tr}\}(\text{OH})\}\text{Cu}$	3.392(1)	3.459(1)	3.331(1), 3.342(1)
$\text{Cu}\{\text{OH}\}_2\text{Cu}$	3.180(1)	3.238(1)	3.009(1)
$\text{Cu}\{\text{OH}\}\text{Cu}$	3.395(1)	3.197(1)	3.248(1), 3.527(1)
$\text{Cu}\{\text{OH}\}\text{Cu}\{\text{OH}\}\text{Cu}$	5.996(1)	5.822(1)	6.006(1)

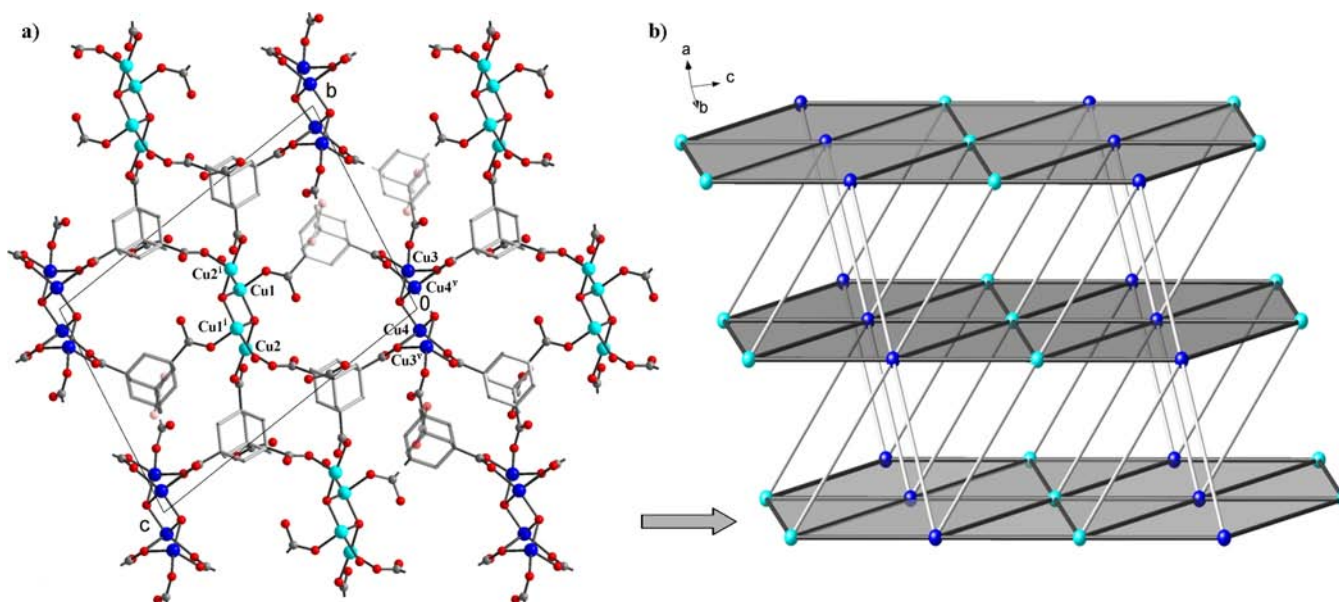


Figure 2. (a) Projection view of the 3D $[\{\text{Cu}_4(\text{OH})_2(\text{H}_2\text{O})_2\}\{\text{Cu}_4(\text{OH})_2\}(\text{H-adtc})_4]_n$ network along the a axis in complex 1 (triazoles are omitted for clarity). (b) Schematic representation of a 8-c uninodal net having a sqc117 topological type: the $\{\text{Cu}_4(\text{OH})_2\}$ SBUs are shown as blue and dark-blue circles to discern A and B types, respectively, while carboxylate links are depicted as gray and light-gray sticks.

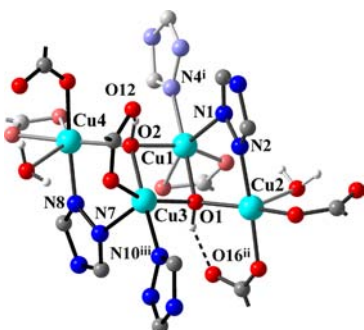


Figure 3. Noncentrosymmetric tetranuclear SBU supported by triazole and hydroxo bridges in compound 2 acting as 6-c nodes of the 2D framework. Symmetry codes: (i) $x - 1, y, z$; (ii) $x, y + 1, z$; (iii) $x + 1, y, z$.

carboxylate groups as well as two water molecules complete the coordination spheres of the copper(II) centers. Two sp^3 -hybridized oxygen atoms, O1 and O2, of μ_3 -OH⁻ are shifted by

0.669 and 0.567 Å each on opposite sides of the mean-square plane of the $\{\text{Cu}_4\}$ core, being oriented toward strong hydrogen-acceptor one-coordinated $-\text{COO}^-$ fragments [$\text{O1} \cdots \text{H} \cdots \text{O16}^{\text{ii}} = 2.571(3)$ Å and $\text{O2} - \text{H} \cdots \text{O12} = 2.701(4)$ Å; Figure 3].

The angular $\text{tr}_{2\text{ad}}$ ligand displays a tridentate role, one triazole group is μ_2 - N^1, N^2 -bridging, and another remains one-coordinated. Thereby, the $\text{tr}_{2\text{ad}}$ ligands provide double links as long as 9.00–9.18 Å between adjacent Cu_4 units along the a direction (Figure 4). Similarly to compound 1, adamantane bistriazole serves as an additional connecting unit, while the adamantane carboxylate acts as a 3-fold-deprotonated tripodal module that organizes the $\{\text{Cu}_4(\text{OH})_2\}$ clusters in the 2D $[\text{Cu}_4(\text{OH})_2(\text{H-adtc})_2]_n$ array. The subtopological motif exists in the form of 2D binodal 3,6-c “Kagomé dual” sheet structure with point symbol $\{4^3\}_2\{4^6.6^6.8^3\}$ (Figure 5).²⁰

The tight packing of hexagonal layers is sustained by means of multiple interlayer hydrogen-bonding interactions of two types that involve noncoordinating carboxylic groups and lattice

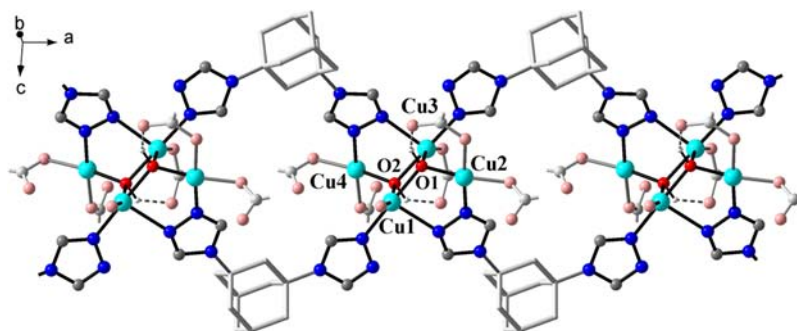


Figure 4. Adamantane bistriazole ligands in **2** that play a bitopic role while using three nitrogen-donor atoms for aligning the tetranuclear fragments along the *a* axis.

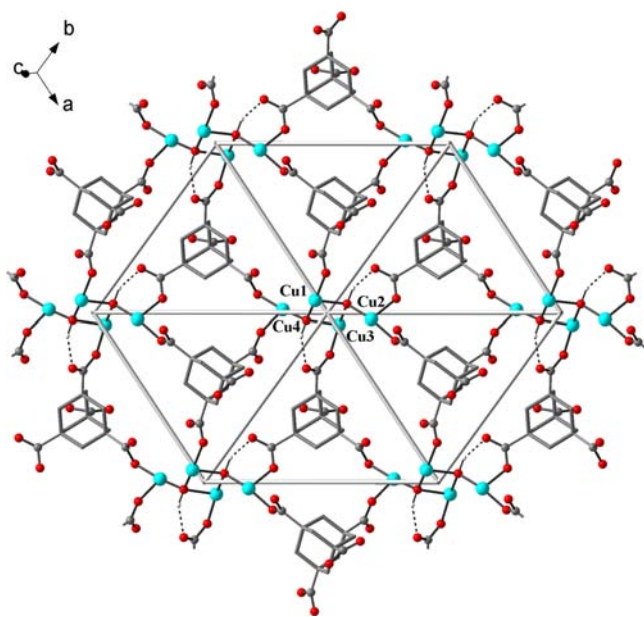


Figure 5. 3-fold-deprotonated carboxylate ligands (H-adtc^{3-}) acting as tripodal spacers organizing the tetranuclear SBUs into the neutral hexagonal framework **2** with a 3,6-topological type.

water molecules as well as carboxylate hydrogen-acceptor fragments, as shown in Figure 6.

A close inspection of the $\{\text{Cu}_4(\text{OH})_2\}$ cluster shell configurations shown in Table 2 reveals the obvious presence of six coordinating carboxylate moieties (e.g., either six pivalate or two triply charged trimesate anions), with the only two exceptions being entry nos. 3 and 4. This suggests that the maintenance of the charge balance is the essential factor to understanding the reason for the more favorable neutral array, as is demonstrated in our case with a $[\text{Cu}_4(\text{OH})_2]^{6+}$ to H-adtr^{3-} carboxylate ratio of 1:2. We propose that the 3-fold-deprotonated H-adtc^{3-} counteranions formed in **1** and **2** can balance the 6^+ -charged SBUs with the carboxylate anions. As previously shown, the dinuclear species (Cu_2^{4+} or Zn_2^{4+}) easily associate with fully deprotonated adtc^{4-} ligands, which under similar reaction conditions results in neutral MOF-11^{4b} and MOF-35,^{4c} both having a microporous nature. In general, 4-fold charged dinuclear units supported by short triazole bridges are more common precedents for Co^{II} than for Cu^{II} .²³ To the best of our knowledge, more recent studies show a close structural relationship between the tetranuclear $\{\text{Cu}_4(\text{OH})_2\}$ and $\{\text{Co}_4(\text{OH})_2\}$ motifs.²⁴

Thermal Stability. The thermal behavior of complexes **1** and **2** were studied using temperature-dependent powder X-ray diffractometry (TD PXRD) in a capillary under an argon atmosphere and DTA. Complex **1** is thermally stable up to 240 °C. In the temperature interval of 130–160 °C, the compound undergoes an interesting phase transition (Figure S18 in the SI). According to DTA/TG, the process can be associated with thermal dehydration that starts at 155 °C. A weight loss of three water molecules is complete by 230 °C (2.50% observed; 2.41% calculated). Above this temperature, the next decomposition step is followed by a gradual release of CO_2 (m/z 44), H_2O (m/z 18), and organic components (Figure S20 in the SI).

Compound **2** remains intact until 180 °C, while further thermal treatment causes changes in the crystal structure that are displayed in the TD PXRD results. The TG curve shows a first mass loss of 5.6% in the temperature interval of 120–190 °C that corresponds to a loss of five water molecules (theoretical weight loss 5.9%) accompanied by an endothermic effect with a peak maximum at 165 °C (Figure 7). This thermal effect causes a structural change that is well correlated with the TD PXRD data (Figure 8). At 260 °C, a significant mass loss is observed (about 22.9%), and above 280 °C, the compound gets amorphous.

Magnetic Properties. The two-dimensionally extended network compound **2** consisting of tetranuclear $\{\text{Cu}_4(\mu_3\text{-OH})_2\}$ core units (type C) was selected for an investigation of its magnetic properties. The magnetic susceptibility data for the polycrystalline sample are displayed as plots of $\chi_m T$ versus T and $1/\chi_m$ versus T in Figures 9 and 10 and as χ_m versus T in Figure S21 in the SI. Upon cooling, compound **2** shows increasing magnetic susceptibility with values from $0.0053 \text{ cm}^3 \text{ mol}^{-1}$ (300 K) to $0.132 \text{ cm}^3 \text{ mol}^{-1}$ (1.9 K). It is worth noting that the $\chi_m T$ versus T plot exhibits decreasing $\chi_m T$ values upon cooling starting with $1.58 \text{ cm}^3 \text{ K mol}^{-1}$ (300 K), reaching a slightly declining plateau at about $0.8 \text{ cm}^3 \text{ K mol}^{-1}$ (around 50 K) before decreasing sharply to $0.22 \text{ cm}^3 \text{ K mol}^{-1}$ (1.9 K), which indicates (i) overall antiferromagnetic exchange interactions among the paramagnetic copper(II) centers and (ii) a diamagnetic ground state for the network compound. As a point of reference, the theoretical $\chi_m T$ value for four magnetically isolated copper(II) ions is $1.58 \text{ cm}^3 \text{ K mol}^{-1}$ ($g = 2.1$). Importantly, the detailed analysis will show (vide infra) that the data taken from room temperature to about 50 K represent mainly the characteristics of the magnetic exchange interactions within a tetranuclear cluster unit, hence leading to a paramagnetic ground state, while describing essentially an isolated cluster unit. Then, at even lower temperatures, only the combined actions of intercluster antiferromagnetic interactions

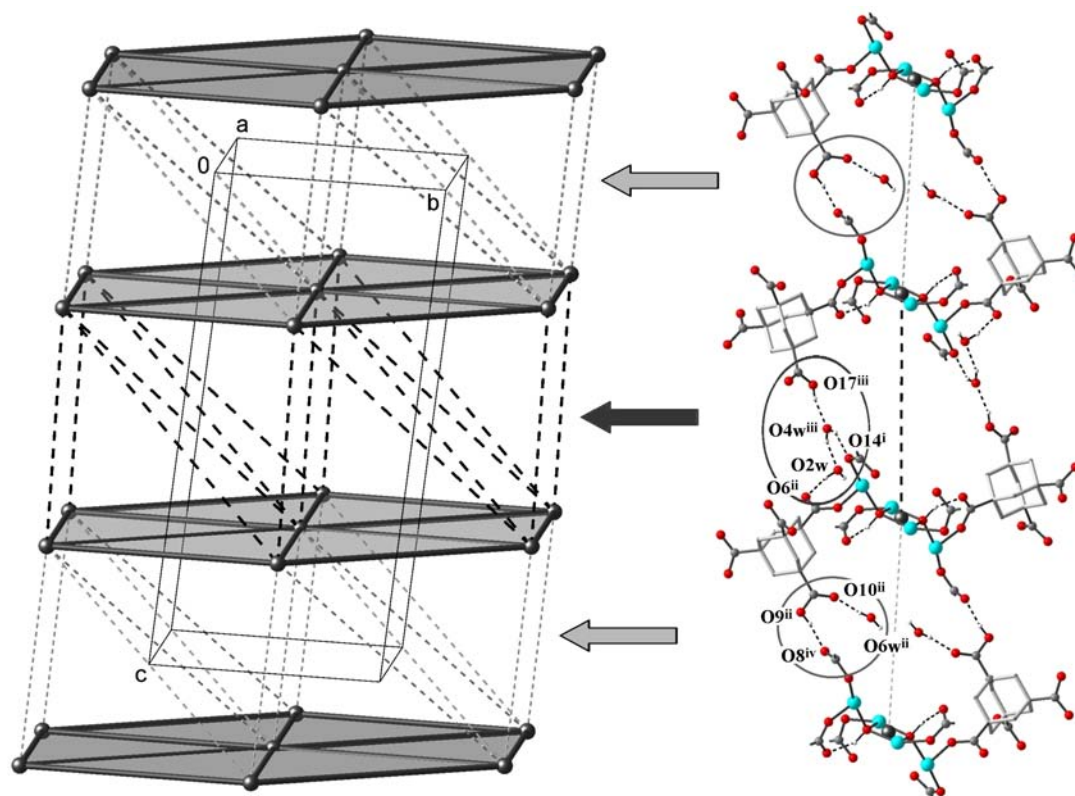


Figure 6. Schematic illustration of the distorted hexagonal packing of $[\text{Cu}_4(\text{OH})_2(\text{H-adt})_2]_n$ (fragment of **2**) showing two kinds of hydrogen-bonding interactions between the neighboring layers: $\text{C}(\text{O})\text{OH}\cdots\text{OC}(\text{O})$ pairs and $\text{C}(\text{O})\text{OH}\cdots\text{OH}_2\cdots\text{OC}(\text{O})$ sequences (light- and dark-gray dashed lines, respectively). Symmetry codes: (i) $x - 1, y, z$; (ii) $x, y - 1, z$; (iii) $-x + 1, -y, -z + 1$; (iv) $-x + 1, -y + 1, -z + 2$.

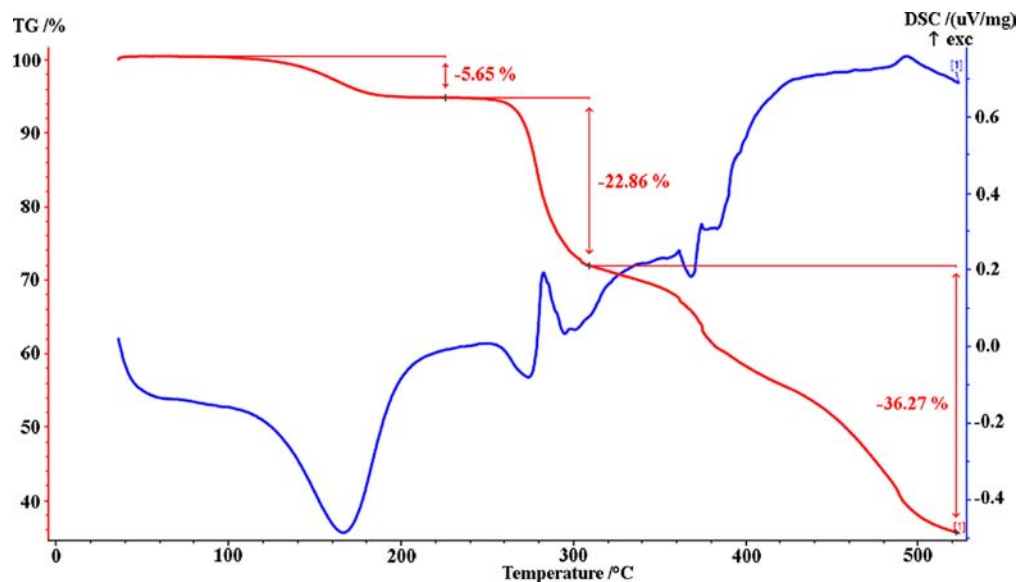


Figure 7. DTA and TG data showing a weight loss (5.6%) in the range 120–190 °C, consistent with the removal of five water molecules for **2**.

and zero-field-splitting effects will finally lead to the distinct drop of the $\chi_m T$ values, expressing the diamagnetic ground state of the network compound as a whole. The inverse magnetic susceptibility curve shows a linear behavior in the temperature range from 200 to 300 K, which results in a Weiss constant $\Theta = -200$ K, in good agreement with the negative slope of the $\chi_m T$ versus T curve.

Given the butterfly-type arrangement of the tetranuclear cluster fragment (Scheme 1), we can use the following isotropic

Hamiltonian to describe the intracluster magnetic exchange interactions (eq 1).

$$H = -2J_1(S_1 \cdot S_3) - 2J_2(S_1 \cdot S_2 + S_1 \cdot S_4 + S_2 \cdot S_3 + S_3 \cdot S_4) \quad (1)$$

This model avoids an overparameterization and approximates the $[\text{Cu}_4]$ core with rhombic symmetry, causing two relevant magnetic exchange pathways, namely, Cu1-Cu3 (J_1) and Cu1-Cu2 , Cu1-Cu4 , Cu2-Cu3 , and Cu3-Cu4 (J_2).

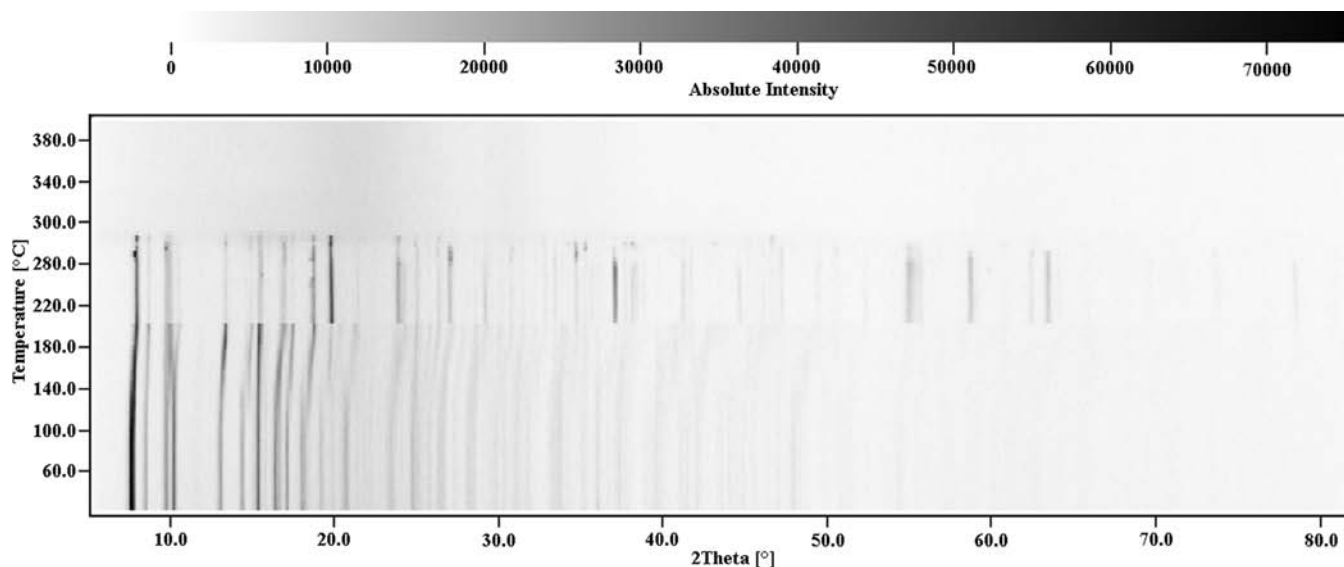


Figure 8. Thermo-PXRD pattern ($2\theta = 5\text{--}80^\circ$) for complex 2, revealing a framework stability of up to 200 °C.

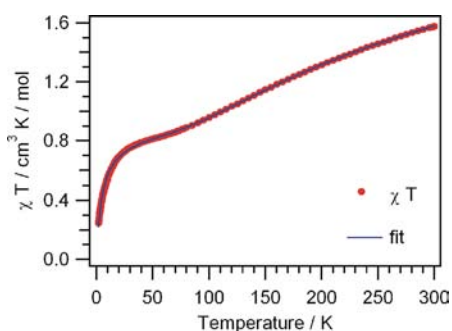


Figure 9. Thermal variation of $\chi_m T$ for 2 (the solid line is a fit according to eq 2, including a mean-field term).

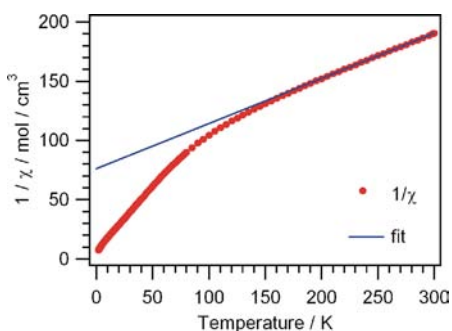


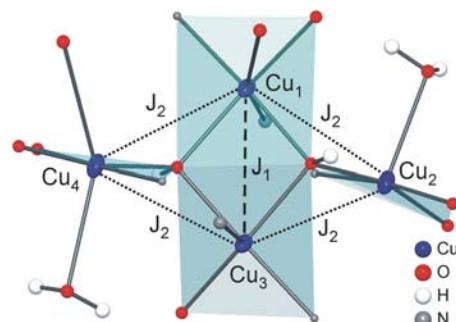
Figure 10. Inverse magnetic susceptibility versus temperature for 2 (the solid line represents a Curie-Weiss fit in the temperature range 200–300 K).

Consequently, the Hamiltonian gives rise to six spin states comprising the total spin values (S_T) of 2, 1, and 0 with the corresponding energy levels in terms of the magnetic coupling constants as given below:

$$E_1(S_T = 2) = -\frac{1}{2}J_1 - 2J_2$$

$$E_2(S_T = 1) = -\frac{1}{2}J_1 + 2J_2$$

Scheme 1. $\{\text{Cu}_4(\mu_3\text{-OH})_2\}$ Core Fragment of 2 and the Corresponding Magnetic Coupling Scheme^a



^aThe planes of the magnetic orbitals are highlighted.

$$E_3(S_T = 1) = -\frac{1}{2}J_1$$

$$E_4(S_T = 1) = +\frac{3}{2}J_1$$

$$E_5(S_T = 0) = -\frac{1}{2}J_1 + 4J_2$$

$$E_6(S_T = 0) = +\frac{3}{2}J_1$$

Applying these energy values to the van Vleck equation gives the following analytical expression (eq 2):

$$\chi_m = 2N\beta^2 g^2 / kT (A/B) \quad (2)$$

$$A = 5 \exp(-E_1/kT) + \exp(-E_2/kT) + \exp(-E_3/kT) + \exp(-E_4/kT)$$

and

$$B = 5 \exp(-E_1/kT) + 3 \exp(-E_2/kT) + 3 \exp(-E_3/kT) + 3 \exp(-E_4/kT) + \exp(-E_5/kT) + \exp(-E_6/kT)$$

In a straightforward manner, it can be deduced that with physically meaningful parameters (g , J_1 , and J_2) the experimental magnetic susceptibility data can be well represented to about 50 K. In this lower temperature regime, de facto only two states will be populated, namely, those with $S_T = 0$ and 1, each at the energy level $+^3/2J_1$. This situation is reflected in the appearance of the slightly declining plateau in the $\chi_m T$ versus T plot. However, the distinct decrease of the $\chi_m T$ values at temperatures below 50 K has its origin in antiferromagnetic intercluster couplings and the zero-field splitting of the $S_T = 1$ state. These effects can be taken into account, although they are different in their physical origin, while combining them into an additional mean-field term, where zj represents the intercluster coupling (eq 3):

$$\chi_m' = \chi_m / [1 - (2zj/N\beta^2 g^2) \chi_m] \quad (3)$$

Using eq 3, the experimental data were fitted satisfactorily in the temperature range 300–1.9 K and best-fit parameters are $g = 2.13$, $J_1 = -109 \text{ cm}^{-1}$, $J_2 = -21 \text{ cm}^{-1}$, and $zj = -2.5 \text{ cm}^{-1}$. The values of the coupling constants express the fairly strong antiferromagnetic intracluster coupling and weak antiferromagnetic interactions between neighboring clusters within the extended network. However, magnetization measurements showed no sign of a magnetic ordering effect to 2 K. The intracluster parameters can, to some extent, be correlated to the molecular structure of the $\{\text{Cu}_4(\mu_3\text{-OH})_2\}$ core unit. On the basis of the evaluation of the bond lengths of the four copper(II) coordination environments in compound **2**, basal planes can be described that reveal that all four magnetic orbitals of the four spin centers are aligned with the Cu–O bonds stemming from the $\mu_3\text{-OH}$ bridges. This situation defines the relevant magnetic exchange pathways between the copper(II) centers and leaves the axially long bond pathways as negligible. The corresponding six short Cu–O bond distances lie in the range of 1.956–2.026 Å, and their slight variation in length will average out while approximating the $[\text{Cu}_4]$ core with rhombic symmetry (Scheme 1). Furthermore, it can be seen that the two “inner” bond angles Cu1–O1–Cu3 (99.1°) and Cu1–O2–Cu3 (97.7°) are distinctly smaller than the four “outer” bond angles Cu1–O1–Cu2 (117.3°), Cu2–O1–Cu3 (110.6°), Cu1–O2–Cu4 (123.2°), and Cu3–O2–Cu4 (114.8°), but in total they show a wide distribution in their values, a fact that will defeat a detailed discussion on a structure–property correlation. Thus, the big picture has to focus on the view that Cu1 and Cu3 are connected through a double μ_3 -hydroxide bridge, which will give more weight to the two “inner” exchange pathways, which act in combination and are jointly parametrized with $J_1 = -109 \text{ cm}^{-1}$, compared to the four “outer” pathways, measured with $J_2 = -21 \text{ cm}^{-1}$, and which reflect only a single μ_3 -hydroxide bridge each. The herein evaluated value $J_1 = -109 \text{ cm}^{-1}$ compares favorably with the one from an analogous structure type;²⁵ however, by contrast most of the reported similar tetranuclear copper(II) complexes place their double μ_3 -hydroxide exchange pathways along one of the elongated bond distances, hence orthogonal to the magnetic orbitals, which consequently will lead to a very different situation with respect to the intracluster magnetic exchange interactions; that is an important point to bear in mind while comparing literature values.

Because of the fact that compound **1** shows two different cluster cores (types A and B) within its structural motif, analysis

of the different magnetic coupling behaviors would clearly lead to an overparameterization of the model.

CONCLUSION

Summarizing the above results, we show that the building-block combination of bitopic 1,2,4-triazol-4-yl and rigid 1,3,5,7-adamantanetetracarboxylate ligands broadens the scope of the mixed-ligand approach in the design of Cu^{II} MOFs, thus integrating discrete tetranuclear coordination clusters into extended networks. The N^1, N^2 -tr heterocycle and *syn, syn*-coordinating carboxylic group serve as self-complementary short bridges that support the formation of tetranuclear $\{\text{Cu}_4(\text{OH})_2\}$ cores. The $\{\text{Cu}_4(\text{OH})_2\}$ configurations are very sensitive to the ligand-type arrangements, which are mostly differentiated by coordination modes of $-\text{COO}^-$, tr, as well as water molecules presented in the cluster shell. Being a potentially tetrapotic building block, 1,3,5,7-adamantanetetracarboxylate acts just as a tripodal three-charged anion H-adtc^{3-} linking the $\{\text{Cu}_4(\text{OH})_2\}$ SBUs in the parent 3,6-subtopological type networks. However, the topology can be elegantly tuned while employing **tr₂ad** with a large bulky adamantane scaffold versus **tr₂pr** with a flexible linear spacer.

A study about the magnetic properties of **2** revealed an interesting situation where the intracluster magnetic exchange interactions lead to a paramagnetic ground state for the discrete $\{\text{Cu}_4(\text{OH})_2\}$ units, which, however, then couple within the extended framework so that at lower temperatures their magnetic moments get canceled in the bulk phase.

ASSOCIATED CONTENT

Supporting Information

X-ray crystallographic data of **1** and **2** in CIF format, crystallographic data and experimental details for X-ray structural analyses, spectral characterization data, thermo-PXRD patterns, and TG-MS analysis. This material is available free of charge via the Internet at <http://pubs.acs.org>.

AUTHOR INFORMATION

Corresponding Author

*E-mail: ab_lysenko@univ.kiev.ua (A.B.L.), liu@iac.unibe.ch (S.-X.L.).

Notes

The authors declare no competing financial interest.

ACKNOWLEDGMENTS

Financial support by Deutsche Forschungsgemeinschaft and by the Swiss National Science Foundation (Grant 200020-130266) is gratefully acknowledged.

REFERENCES

- (1) (a) Perry, J. J., IV; Perman, J. A.; Zaworotko, M. J. *Chem. Soc. Rev.* **2009**, *38*, 1400. (b) Tranchemontagne, D. J.; Mendoza-Cortés, J. L.; O’Keeffe, M.; Yaghi, O. M. *Chem. Soc. Rev.* **2009**, *38*, 1257.
- (2) (a) Janiak, C. *Dalton Trans.* **2003**, 2781. (b) Kepert, C. J. *Chem. Commun.* **2006**, 695. (c) O’Keeffe, M.; Yaghi, O. M. *Chem. Rev.* **2012**, *112*, 675. (d) Eddaoudi, M.; Moler, D. B.; Li, H.; Chen, B.; Reineke, T. M.; O’Keeffe, M.; Yaghi, O. M. *Acc. Chem. Res.* **2001**, *34*, 319.
- (3) Silver, cadmium, manganese, zinc, cobalt, and copper adamantanedicarboxylate: (a) Jin, J.-C.; Wang, Y.-Y.; Zhang, W.-H.; Lermontova, A. S.; Lermontova, E. Kh.; Shi, Q.-Z. *Dalton Trans.* **2009**, 10181. (b) Jin, J.-C.; Wang, Y.-Y.; Liu, P.; Liu, R.-T.; Ren, C.; Shi, Q. Z. *Cryst. Growth Des.* **2010**, *10*, 2029. (c) Zhang, J.; Chen, Sh.; Nieto, R. A.; Wu, T.; Feng, P.; Bu, X. *Angew. Chem., Int. Ed.* **2010**, *49*, 1267.

- (d) Nielsen, R. B.; Kongshaug, K. O.; Fjellvåg, H. *J. Mater. Chem.* **2008**, *18*, 1002. (e) Xu, D. J.; Pan, L.; Emge, T. J.; Huang, X.-Y.; Li, J. *Acta Crystallogr.* **2006**, *C62*, m150. Lanthanum, thorium, uranium and adamantanedicarboxylate: (f) Millange, F.; Serre, C.; Marrot, J.; Gardant, N.; Pellé, F.; Férey, G. *J. Mater. Chem.* **2004**, *14*, 642. (g) Nazarenko, O. M.; Rusanova, J. A.; Krautscheid, H.; Domasevitch, K. V. *Acta Crystallogr.* **2010**, *C66*, m276. (h) Ok, K. M.; O'Hare, D. *Dalton Trans.* **2008**, 5560. (i) Rusanova, J. A.; Rusanov, E. B.; Domasevitch, K. V. *Acta Crystallogr.* **2010**, *C66*, m207.
- (4) Zinc, cadmium, nickel, and copper adamantanetetracarboxylates: (a) Rosi, N. L.; Kim, J.; Eddaoudi, M.; Chen, B.; O'Keeffe, M.; Yaghi, O. M. *J. Am. Chem. Soc.* **2005**, *127*, 1504. (b) Kim, J.; Chen, B.; Reineke, T. M.; Li, H.; Eddaoudi, M.; Moler, D. B.; O'Keeffe, M.; Yaghi, O. M. *J. Am. Chem. Soc.* **2001**, *123*, 8239. (c) Chen, B.; Eddaoudi, M.; Reineke, T. M.; Kampf, J. W.; O'Keeffe, M.; Yaghi, O. M. *J. Am. Chem. Soc.* **2000**, *122*, 11559.
- (5) Taylor, J. M.; Mahmoudkhani, A. H.; Shimizu, G. K. H. *Angew. Chem., Int. Ed.* **2007**, *46*, 795.
- (6) (a) Hoffart, D. J.; Dalrymple, S. A.; Shimizu, G. K. H. *Inorg. Chem.* **2005**, *44*, 8868. (b) Hoffart, D. J.; Côté, A. P.; Shimizu, G. K. H. *Inorg. Chem.* **2003**, *42*, 8603.
- (7) (a) Senchyk, G. A.; Lysenko, A. B.; Rusanov, E. B.; Chernega, A. N.; Krautscheid, H.; Domasevitch, K. V. *Inorg. Chim. Acta* **2009**, *362*, 4439. (b) Lysenko, A. B.; Senchyk, G. A.; Lincke, J.; Lässig, D.; Fokin, A. A.; Butova, E. D.; Schreiner, P. R.; Krautscheid, H.; Domasevitch, K. V. *Dalton Trans.* **2010**, 39, 4223. (c) Senchyk, G. A.; Lysenko, A. B.; Boldog, I.; Rusanov, E. B.; Chernega, A. N.; Krautscheid, H.; Domasevitch, K. V. *Dalton Trans.* **2012**, 8675.
- (8) (a) Haasnoot, J. G. *Coord. Chem. Rev.* **2000**, *200*, 131. (b) Klingele, M. H.; Brooker, S. *Coord. Chem. Rev.* **2003**, *241*, 119. (c) Beckmann, U.; Brooker, S. *Coord. Chem. Rev.* **2003**, *245*, 17. (d) Aromía, G.; Barrios, L. A.; Roubeaub, O.; Gameza, P. *Coord. Chem. Rev.* **2011**, *255*, 485.
- (9) Kahn, O. *Molecular Magnetism*; VCH: Weinheim, Germany, 1993.
- (10) Yang, E.-C.; Liu, Z.-Y.; Shi, X.-J.; Liang, Q.-Q.; Zhao, X.-J. *Inorg. Chem.* **2010**, *49*, 7969.
- (11) (a) Garcia, Y.; van Koningsbruggen, P. J.; Kooijman, H.; Spek, A. L.; Haasnoot, J. G.; Kahn, O. *Eur. J. Inorg. Chem.* **2000**, 307. (b) Zilverentant, C. L.; Driessen, W. L.; Haasnoot, J. G.; Kolnaar, J. J. A.; Reedijk, J. *Inorg. Chim. Acta* **1998**, *282*, 257. (c) Habib, H. A.; Sanchiz, J.; Janiak, C. *Dalton Trans.* **2008**, 1734. (d) Garcia, Y.; Bravic, G.; Gieck, C.; Chasseau, D.; Tremel, W.; Gülich, P. *Inorg. Chem.* **2005**, *44*, 9723. (e) Pilkington, M.; Decurtins, S. *Chimia* **2000**, *54*, 593. (f) Decurtins, S.; Schmalle, H. W.; Pellaux, R.; Huber, R.; Fischer, P.; Ouladdiaf, B. *Adv. Mater.* **1996**, *8*, 647. (g) Bonadiao, F.; Senna, M.-C.; Enslin, J.; Sieber, A.; Neels, A.; Stoeckli-Evans, H.; Decurtins, S. *Inorg. Chem.* **2005**, *44*, 969.
- (12) Lee, G. S.; Bashara, J. N.; Sabih, G.; Oganessian, A.; Godjoian, G.; Duong, H. M.; Marinez, E. R.; Gutierrez, C. G. *Org. Lett.* **2004**, *6*, 1705.
- (13) Sheldrick, G. M. *Acta Crystallogr.* **2008**, *A64*, 112.
- (14) (a) Yang, E.-C.; Zhang, C.-H.; Liu, Z.-Y.; Zhang, N.; Zhao, L.-N.; Zhao, X.-J. *Polyhedron* **2012**, *40*, 65. (b) Li, W.; Li, M.-X.; Shao, M.; Wang, Z.-X.; Liu, H.-J. *Inorg. Chem. Commun.* **2008**, *11*, 954. (c) Meng, Z.-S.; Yun, L.; Zhang, W.-X.; Hong, C.-G.; Herchel, R.; Ou, Y.-C.; Leng, J.-D.; Peng, M.-X.; Lin, Z.-J.; Tong, M.-L. *Dalton Trans.* **2009**, 10284. (d) Qiao, L.-Y.; Zhang, J.; Li, Z.-J.; Qin, Y.-Y.; Cheng, J.-K.; Yao, Y.-G. *J. Mol. Struct.* **2005**, *994*, 1.
- (15) Zhou, J.-H.; Cheng, R.-M.; Song, Y.; Li, Y.-Z.; Chen, X.-T.; Xue, Z.-L.; You, X.-Z. *Inorg. Chem.* **2005**, *44*, 8011.
- (16) Yang, E.-C.; Yang, Y.-L.; Liu, Z.-Y.; Liu, K.-S.; Wu, X.-Y.; Zhao, X.-J. *CrystEngComm* **2011**, *13*, 2667.
- (17) Yang, E.-C.; Ding, B.; Liu, Z.-Y.; Yang, Y.-L.; Zhao, X.-J. *Cryst. Growth Des.* **2012**, *12*, 1185.
- (18) Habib, H. A.; Sanchiz, J.; Janiak, C. *Inorg. Chim. Acta* **2009**, *362*, 2452.
- (19) Senchyk, G. A.; Lysenko, A. B.; Krautscheid, H.; Sieler, J.; Domasevitch, K. V. *Acta Crystallogr.* **2008**, *C64*, m246.
- (20) (a) Blatov, V. A. *TOPOS IUCr CompComm Newsletter* **2006**, *7*, 4. (b) Blatov, V. A.; Shevchenko, A. P.; Serezhkin, V. N. *J. Appl. Crystallogr.* **2000**, *33*, 1193.
- (21) The EPINET database: <http://epinet.anu.edu.au/sqc117>.
- (22) Addison, A. W.; Rao, T. N.; Reedijk, J.; Rijn, J. V.; Verschoor, G. C. *J. Chem. Soc., Dalton Trans.* **1984**, 1349.
- (23) (a) Vos, G.; Haasnoot, J. G.; Verschoor, G. C.; Reedijk, J. *Inorg. Chim. Acta* **1985**, *102*, 187. (b) Engelfriet, D. W.; Verschoor, G. C.; den Brinker, W. *Acta Crystallogr.* **1980**, *B36*, 1554. (c) Yoo, H. S.; Lim, J. H.; Kang, J. S.; Koh, E. K.; Hong, C. S. *Polyhedron* **2007**, *26*, 4383.
- (24) (a) Mahata, P.; Natarajan, S.; Panissod, P.; Drillon, M. *J. Am. Chem. Soc.* **2009**, *131*, 10140. (b) Lama, P.; Aijaz, A.; Sañudo, E. C.; Bharadwaj, P. K. *Cryst. Growth Des.* **2010**, *10*, 283. (c) Ji, J.-W.; Zhang, W.; Zhang, G.-X.; Han, Z.-B. *Inorg. Chem. Commun.* **2009**, *12*, 956. (d) Ahmad, M.; Sharma, M. K.; Das, R.; Poddar, P.; Bharadwaj, P. K. *Cryst. Growth Des.* **2012**, *12*, 1571. (e) Chen, Q.; Xue, W.; Lin, J.-B.; Lin, R.-B.; Zeng, M.-H.; Chen, X.-M. *Dalton Trans.* **2012**, 4199. (f) Luo, J.; Zhao, Y.; Xu, H.; Kinnibrugh, T. L.; Yang, D.; Timofeeva, T. V.; Daemen, L. L.; Zhang, J.; Bao, W.; Thompson, J. D.; Currier, R. P. *Inorg. Chem.* **2007**, *46*, 9021. (g) Sarma, D.; Srivastava, V.; Natarajan, S. *Dalton Trans.* **2012**, 4135.
- (25) Zhang, R.-B.; Zhang, J.; Li, Z.-J.; Cheng, J.-K.; Qin, Y.-Y.; Yao, Y.-G. *Cryst. Growth Des.* **2008**, *8*, 3735.